fire

MDPI

Article

Study on the Control Effect of Borehole Gas Extraction in Coal Seams Based on the Stress–Seepage Coupling Field

Hongsheng Wang [1], Huaming An [2,3,*] and Bingbing Yang [2]

[1] Beijing Chemical Occupational Disease Prevention and Control Institute, Beijing 100093, China
[2] Faulty of Public Security and Emergency Management, Kunming University of Science and Technology, Kunming 650093, China
[3] Geotechnical Institute, TU Bergakademie Freiberg, 09599 Freiberg, Germany
* Correspondence: huaming.an@kust.edu.cn

Abstract: In order to determine the reasonable parameters of high-gas and extra-thick coal seam drainage, considering the factors of the coal seam metamorphic degree, stress condition, gas occurrence state, and permeability dynamic change, the gas desorption, diffusion, and transport process of coal seam gas are analyzed. A secondary distribution model of coal around the borehole, a porosity variation model of coal around the borehole, a stress–seepage coupling model, a pore flow model of the pressure-driven transition flow zone, and a free molecular flow zone are established. Taking the gas drainage of Zhangcun Coal Mine of Lu'an Group as the research object, the influence of drilling hole diameter, coal seam permeability, gas original pressure, and other factors on the control range of coal seam drainage drilling is simulated by ANSYS Fluent 6.3.26. The results show that secondary stress distribution occurs in the coal seam drill hole under the action of lead stress, which leads to the change in porosity; the seepage zone, transition zone, molecular flow zone, and original rock stress zone are presented around the drill hole; and the range of influence of the drill hole is mainly based on the seepage zone and the transition zone, supplemented by the molecular flow zone. The control range of the drill hole is in a positive proportional relationship to the diameter of the drill hole, the porosity of the coal seam, and the original pressure of the gas.

Keywords: stress field; seepage field; multi-field coupling; pumping control range; numerical simulation

Citation: Wang, H.; An, H.; Yang, B. Study on the Control Effect of Borehole Gas Extraction in Coal Seams Based on the Stress–Seepage Coupling Field. *Fire* **2024**, *7*, 410. https://doi.org/10.3390/fire7110410

Academic Editors: Chuyuan Huang, Haipeng Jiang and Lijuan Liu

Received: 3 October 2024
Revised: 21 October 2024
Accepted: 28 October 2024
Published: 8 November 2024

1. Introduction

As an important basic energy source for China's economic and social development, coal has made remarkable progress both in terms of the scope and intensity of its exploitation. Coal plays an indispensable role in national economic development and modernization. With the development of the national economy and the continuous progress of science and technology, large-scale mega coal mines have been put into operation one after another, and the coal mining method has shifted from traditional artillery mining and general mining to synthesis mining, which has a higher efficiency. The depth record of coal seams has been broken continuously, and the high pressure and content of coal seam gas has become one of the important characteristics of modern coal mining. According to the requirements of the relevant laws and regulations, high-gas mines must extract the coal seam gas before mining, so that the coal seam gas pressure and content can be reduced to the mining requirements. However, in the case of high-gas and extra-thick coal seam integrated mining, the high mining intensity, the high coal residue in the hollow mining area, and the high gas content in the neighboring layers and surrounding rocks make it very easy for the integrated working face to have the phenomenon of gas exceeding the limitation, which may lead to gas explosions, gas asphyxiation, and other disasters and bring a great safety hazard to the production of the mines.

Since the first synthesized working face was put to the test in China in 1984, the technology of synthesized-roof coal mining has been developed rapidly. At present, the working faces of integrated-roof coal mining in China are among the top in the world in terms of the number and scope of use, the advancement of technology, and the results achieved. However, with the increase in demand for coal and the improvement in production technology, coal seams mined by integrated-roof coal mining are gradually characterized by their high gas and high protrusion levels. At the same time, production practices have also gradually exposed the many hidden disasters or dangers of comprehensive roof coal mining technology, such as a high absolute gas outflow, frequent spontaneous combustion and fire, and other problems, and this approach has triggered a number of various types of major disasters and accidents. It is easy to see that gas accidents have become one of the most serious types of accidents in China's coal mines, and the number of deaths in gas accidents (such as gas explosions, coal and gas protrusion, and gas asphyxiation) has been the most common type of large accident for many years.

In recent decades, many scholars have conducted extensive scientific research and production practices on the prevention and control technologies for major gas disasters in comprehensive mining. They have proposed various gas management measures, including: pre-mining gas extraction, gas extraction during tunneling and mining, high-yield drilling for gas extraction, burying pipes in the upper corners for gas discharge, increasing air distribution, and arranging the working face along the roof plate to facilitate gas discharge towards higher-level tunnels. These measures aim to effectively prevent and control gas disasters. Wang et al. [1] determined the effective influence radius of gas extraction by numerical simulation for the reasonable arrangement of gas-extraction boreholes along a coal seam, which provided a basis for the optimization of single gas-extraction boreholes along coal seams. Liu et al. [2] theoretically studied the effective gas-extraction radius of bedding boreholes. Zhao [3] gave full consideration to the technical advantages of high-level roof drilling and improved the hole-forming rate of high-level drilling. Zhu [4] proposed an evaluation method of drilling control effects based on a physical examination method. This method divides a coal seam into several control bodies whose side lengths are equal to the effective radius of extraction and uses computer technology to evaluate the control effect of drilling. In the Hebi mining area, the layout method of using cross boreholes is used to arrange a pair of boreholes every 2.5~3.0 m, in which one hole is parallel to the working face and the other hole is oblique to the working face. The angle between the two holes is 10°~15°, and the aperture is 79 mm. This method has achieved a good drainage effect. These fruitful results provide a basis for mine gas control, reducing the harm of gas in coal mining, and provide a guarantee for safe mine production. However, due to the unpredictability of coal and rock storage conditions and the special nature of production conditions, the prevention and control measures of major disasters often fail to meet the design objectives, such as when the gas pumping effect of the mining area is generally poor, with a low pumping rate. Because serious accidents caused by gas are repeated, resulting in the majority of accidental deaths, the mortality rate per million tons of coal production remains high, a serious threat to the majority of China's coal mine workers' safety, social stability, and unity, causing an extremely negative impact. At the same time, it has also brought significant casualties and property losses to individuals, coal mining enterprises, and the State.

Solving the problem of gas disasters in high-gas synthesized working faces is an urgent task facing us. Multiple accident causative factors, a wide range of hazards, and serious consequences have become the characteristics of roof coal mining in high-gas mines. Therefore, it is necessary to summarize the valuable experience of predecessors on the basis of the current mine production situation, to crack these technical problems, and to provide theoretical support and a technological guarantee for the realization of the development of high-gas comprehensive roof coal mining mines, with the goal of a high output, high efficiency, high effectiveness, and high safety. With the increased application of seepage diffusion theory in the field of coal seam gas drainage and the

continuous deepening and improvement of theoretical research, domestic and foreign experts and scholars have summarized the process of gas transport and its influencing factors through theoretical analysis and experimental research. It has been proven that the gas transportation process is a result of the joint action of multiple factors, such as the geological conditions of the coal seam, the degree of coal body metamorphism, the original pressure of the gas, and the ground stress. However, due to the special nature of its storage conditions, the storage and seepage process of gas is subject to a variety of external forces, such as the ground stress field, ground electric field, ground temperature field, etc., and each of these factors will have different degrees of influence on its flow in a porous medium. Worse still, the coupling of the various fields enhances the likelihood of composite disaster and destruction, which makes the prevention and control become more difficult. In this regard, some scholars have explored and researched the multi-field coupling law of coal seam gas and put forward many fluid–solid coupling models [5–13]. Enever (1997) [14,15] analyzed the relationship between the ground stress and the permeability of a coal seam and obtained an exponentially correlated rule of change between the two. Zhen et al. [16] established a coupled model of stress–seepage damage for hydraulic fracturing of rock bodies. In order to determine the law of temporal and spatial evolution, Jasinge et al. [17] conducted gas permeability testing experiments on coal samples under different enclosing pressures and obtained the law describing the stress–permeability change of Australian lignite coals. Cao et al. [18] established a nonlinear seepage equation of water injection in coal seams by analyzing the stress distribution of the workings and its influence on the characteristics of water injection into coal seams. Zhao et al. [19] established a multi-field (including coal stress field, damage field, gas diffusion field, and seepage field) coupling model based on the non-homogeneity of a coal body. Liu et al. [20] further discussed the characteristics of the dynamic evolution distribution of stress and seepage throughout the coal seam water injection process based on a numerical simulation and experimental results.

In recent years, with the popularization and application of simulation (CFD) software, domestic scholars have carried out simulation research on the air flow field and gas migration in goaf and achieved certain results. Based on CFD simulation software, Yuan et al. [21] systematically studied the dynamic changes in the stress field, fracture field, and gas flow field in the No.11 coal seam of the Guqiao Coal Mine. Based on Fluent simulation software, a three-dimensional heterogeneous numerical model of gas flow in goaf was established by Hu et al., Li et al., and Zhang et al. [22–24]. In a study by Wang et al. [25] based on the Fick diffusion law, Darcy seepage law, and Fourier heat conduction law, a multi-physical field coupling model of goaf considering temperature change was established by using mass conservation and energy conservation equations based on the three-dimensional porosity model. The above researchers have analyzed the mechanism and influencing factors of the multi-field coupling of coal seam gas through coal mine field monitoring, laboratory experiments, and numerical simulation. However, the multi-field coupling mechanism is not yet clear, the relevant prevention and control measures are still not effective, and the research on the stress–seepage coupling field is relatively few. Based on the secondary distribution of stress caused by coal seam drilling, combined with the change in porosity around the borehole, this paper studies the seepage process formed by the coupling of the stress field and seepage field and the void and micro-pore flow process in the pressure-driven transition flow zone and free molecular flow zone [26–29]. According to the secondary distribution characteristics of borehole stress in coal seams, the spatial variation law of permeability around boreholes, and the fluid–solid coupling model of gas, the variation law of the control range of a gas drainage borehole in a high-gas and extra-thick coal seam is simulated by ANSYS Fluent 6.3.26. The research results can provide theoretical reference for the optimal layout of drainage boreholes.

2. Theoretical Analyses and Model Establishment

In this section, the main sources of gas and its transport law in the face of comprehensive mining are studied and analyzed by reviewing relevant information; applying theoretical knowledge and technical methods of geology, mining, fluid mechanics, the gas disaster control principle, the comprehensive roof coal mining process, and other related disciplines; applying the theory of seepage in porous media combined with the actual characteristics of a mined coal seam; and establishing equations of gas desorption, diffusion, and transportation of a coal seam under porous media. The secondary distribution of the stress field in the coal body around the borehole, the change rule of the void degree under the influence of stress–strain, the dynamic model of fluid–solid coupling in the gas pumping process, and the pore flow model of the pressure-driven transition flow zone and free molecular flow zone were determined.

2.1. Theoretical Analyses of Gas Migration Law of Pre-Drainage Coal Seam in Fully Mechanized Caving Face

A coal seam is a dual medium of pore and fracture. Gas exists in the matrix in the form of adsorption. It undergoes the process of desorption from the coal body, diffusion to the pore, and fracture and transport in the coal seam fracture before production [30,31].

1. Coal seam gas desorption

There are three main types of models describing coal seam gas adsorption, namely the Langmuir isothermal adsorption model, potential difference theory model, and Gibbs model [32]. Among them, the Langmuir isothermal adsorption model is the most commonly used:

$$V_E(p) = V_L \frac{p}{p_L + p} \tag{1}$$

where $V_E(p)$ is the adsorption capacity, g/m^3; p is pressure, MPa; V_L is the Langmuir volume, g/m^3; and p_L is the Langmuir pressure, MPa. Langmuir pressure is the pressure when the adsorption capacity reaches 50% of the limit adsorption capacity.

2. Coal seam gas diffusion

Gas diffusion in a coal seam is divided into quasi-steady-state diffusion and non-steady-state diffusion.

(1) Quasi-steady-state diffusion (based on Fick's first law [33,34])

It is believed that the diffusion process of gas in a coal seam can be expressed by the change in the average concentration in each time period being proportional to the difference of time:

$$\frac{dC_m}{dt} = D_m F_s (C_2 - C_m) \tag{2}$$

where:

$$q_m = -G \frac{dC_m}{dt} \tag{3}$$

$$\tau = \frac{1}{D_m F_s} \tag{4}$$

$$F_s = 8\pi / S^2 \tag{5}$$

where C_m is the concentration in the matrix, g/m^3; D_m is the mass diffusion coefficient in porous media, m^2/s; C_2 is the concentration at the edge of the matrix block, g/m^3; F_s is the matrix block shape factor, m^{-2}; q_m is the amount of gas desorption; G is a geometric factor; τ is the adsorption time constant, s; and S is cleat spacing, m.

It can be seen from the above formula that the adsorption time is related to the diffusion distance; that is, it is proportional to the square of the fracture spacing.

(2) Unsteady diffusion (based on Fick's second law [35,36])

It is considered that the diffusion process of gas in the geometric block of the matrix can be described in the form of partial differential equations. Coal seam gas mainly includes two parts: one part is the free gas contained in pores and fractures and the other part is the gas adsorbed on the surface of the matrix. The concentration of free gas is:

$$C_1 = \rho_1 \phi_m = \frac{MP_m \phi_m}{RTZ} \tag{6}$$

The concentration of adsorbed gas is:

$$C_2 = V_L \frac{p}{p_L + p_m} \tag{7}$$

The total gas concentration in the matrix block is:

$$C_m = \frac{MP_m \phi_m}{RTZ} + V_L \frac{p}{p_L + p_m} \tag{8}$$

According to Fick's second diffusion law, the equation of pressure in pores is:

$$\frac{\partial}{\partial t}\left(\frac{MP_m \phi_m}{RTZ} + V_L \frac{p}{p_L + p_m}\right) = \nabla\left[D_m \nabla\left(\frac{MP_m \phi_m}{RTZ} + V_L \frac{p}{p_L + p_m}\right)\right] \tag{9}$$

After the gas concentration is solved by Equations (8) and (9), the amount of gas flowing out of the matrix block is:

$$q_m = -\frac{A_1}{V_1} J = -\frac{A_1}{V_1} D_m \nabla C_m \tag{10}$$

where C_1 is the concentration of free gas, g/m^3; ϕ_m is matrix porosity; C_m is the sum of the concentration of adsorbed gas C_{ma} and free gas C_{mf} in the matrix; p_m is the gas pressure in the pore, MPa; A_1 is the surface area of the matrix block unit, m^2; J is the diffusion flux, g/m^2·s; and V_1 is the volume of matrix block unit, m^3.

3. Coal seam gas transport

Due to the continuous gas diffusion into the cracks in the coal matrix block, it should be regarded as a continuous source distribution in the continuity equation. The mass conservation equation of gas transport in cracks is [37]:

$$\frac{\partial}{\partial t}\left(\phi_f s_{fg} \rho_{fg}\right) = -\nabla \cdot \left(\rho_{fg} V_{fg}\right) + q_m \tag{11}$$

Among them is the quality of the gas that diffuses into the crack. The velocity consists of two parts: the macroscopic seepage velocity following Darcy's law and the diffusion velocity following Fick's law, that is:

$$V_{fg} = -\left(\frac{K_g}{\mu_g} \nabla P_{fg} + \frac{D_f}{C_f} \nabla C_f\right) \tag{12}$$

The density and concentration in Equations (11) and (12) are expressed by pressure, respectively:

$$\rho_{fg} = \frac{M}{RT}\left(\frac{P_{fg}}{Z}\right) \tag{13}$$

When isothermal,

$$\frac{\nabla C_f}{C_f} = \nabla\left(s_{fg} \frac{P_{fg}}{Z}\right) / \left(s_{fg} \frac{P_{fg}}{Z}\right) \tag{14}$$

Equation (11) becomes:

$$\frac{\partial}{\partial t}\left(\frac{\phi_f s_g p_g}{Z}\right) = \nabla \cdot \left[\frac{p_g}{Z}\frac{K_g}{\mu_g}\nabla P_g + \frac{D_f}{s_g}\nabla\left(\frac{s_g p_g}{Z}\right)\right] + \frac{RT}{M}q_m \tag{15}$$

where D_f is the gas diffusion coefficient in the fracture; C_f is the gas concentration in the fracture, $C_f = \phi_f \rho_g$; ϕ_f is the fracture porosity; s_g is the gas saturation; K is the coal seam permeability, m^2; μ is gas viscosity, Pa·s; and m, f, and g represent the matrix, fracture, and gas, respectively.

In summary, a complete description of the coal seam gas output process was described above.

2.2. Establishment of Secondary Distribution Model of Stress Field of Coal Around Borehole

The occurrence of gas disasters is ultimately a process of energy transfer and release. Fully mechanized caving mining destroys the original stress equilibrium state of mining coal seams and breaks the dynamic equilibrium condition of gas adsorption–desorption in a coal seam, resulting in a large amount of adsorbed gas released from mining layer, adjacent layer, and surrounding rock, forming gas accumulation in local space. Due to the drilling construction, the original stress state of the coal seam changes, and the stress of the coal body around the drilling site is redistributed. After the hole is formed, the coal body at the hole wall produces large secondary stress and shear failure. The damaged coal body still bears part of the overburden pressure; however, most of the pressure is transmitted to the external coal body unit and generates concentrated stress, which further damages the coal body. After the stress is balanced, the pressure relief zone, the stress concentration zone, and the original stress zone are formed along the radial direction of the borehole [38].

According to the static equilibrium equation, it can be seen that the equilibrium conditions along the tangential direction of the arc are naturally satisfied for the axisymmetric, volume, and shape-invariant unit body, resulting in shear stress. The components of tangential stress and radial stress in the radius direction are:

$$\left(\sum \sigma_\theta\right)_r = 2\sigma_\theta dr sin\,\frac{d\theta}{2} = \sigma_\theta dr d\theta \tag{16}$$

$$\left(\sum \sigma_r\right)_r = \sigma_r r d\theta - (\sigma_r - d\sigma_r)(r + dr)d\theta \tag{17}$$

From $\left(\sum \sigma_\theta\right)_r + \left(\sum \sigma_r\right)_r = 0$, and by eliminating $d\theta$ and omitting the second-order trace term $dr d\sigma_r$, the static equilibrium differential equation is obtained:

$$r\frac{d\sigma_r}{dr} + \sigma_r - \sigma_\theta = 0 \tag{18}$$

Using geometric equations and physical equations to solve Equation (18):

$$\begin{cases} r\frac{d\sigma_r}{dr} + \sigma_r - \sigma_\theta = 0 \\ \varepsilon_r = \frac{du}{dr} \\ \varepsilon_\theta = \frac{u}{r} \\ \varepsilon_z = 0 \\ \sigma_z = \mu(\sigma_\theta + \sigma_r) \\ \varepsilon_r = \frac{1-\mu^2}{E}(\sigma_r - \frac{\mu}{1-\mu}\sigma_\theta) \\ \varepsilon_\theta = \frac{1-\mu^2}{E}(\sigma_\theta - \frac{\mu}{1-\mu}\sigma_r) \end{cases} \tag{19}$$

There are:

$$\frac{d^2\sigma_r}{dr^2} + \frac{3}{r}\frac{d\sigma_r}{dr} = 0 \tag{20}$$

Combined with boundary conditions:

$$\begin{cases} \sigma_r = p & r \to \infty \\ \sigma_r = 0 & r = a \end{cases} \tag{21}$$

The solution of Equation (20) is:

$$\begin{cases} \sigma_r = p(1 - \frac{a^2}{r^2}) \\ \sigma_\theta = p(1 + \frac{a^2}{r^2}) \end{cases} \tag{22}$$

where σ_θ is the tangential stress, MPa; σ_r is the radial stress, MPa; r is the stress radius, m; a is the diameter of the borehole, m; and p is the original rock stress, MPa.

According to Equation (22), the range of secondary stress distribution around boreholes with different apertures can be obtained, and the change curve is shown in Figure 1a–d.

(**a**)

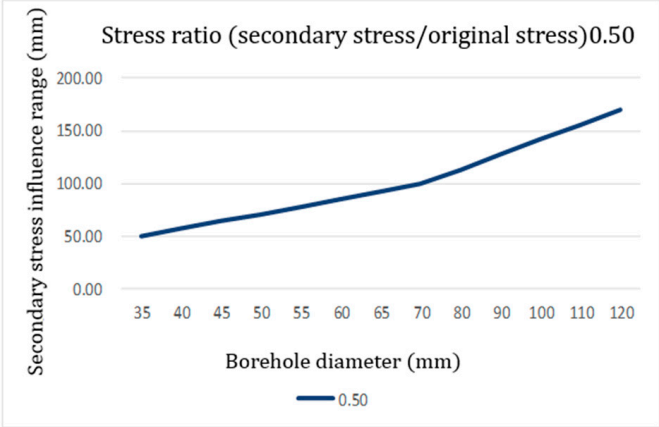

(**b**)

Figure 1. *Cont.*

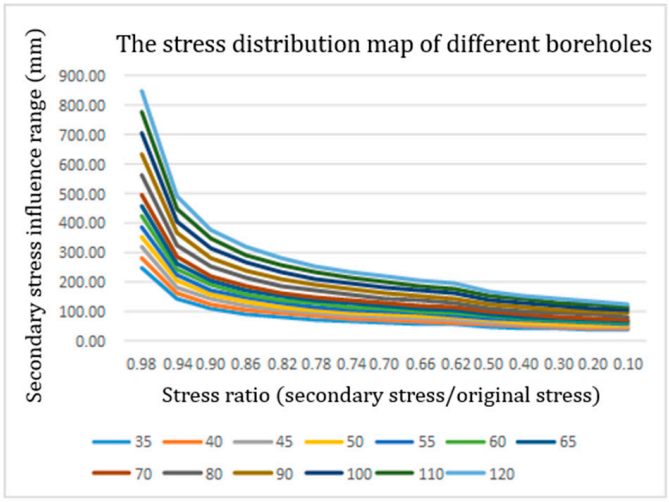

(**c**)

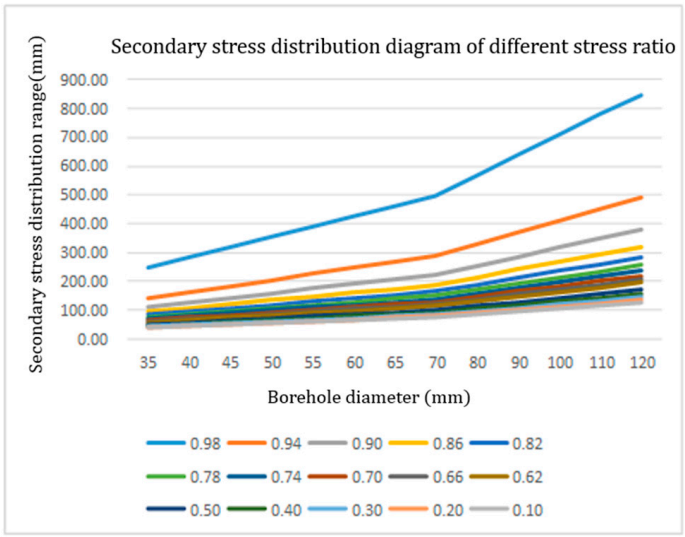

(**d**)

Figure 1. (**a**) The secondary stress distribution around the borehole with a diameter of 60 mm. (**b**) Secondary stress distribution map around the borehole at a stress ratio of 0.5. (**c**) Secondary stress distribution around different boreholes. (**d**) Secondary stress distribution around boreholes with different stress ratios.

Figure 1a shows that when the diameter of the borehole is constant, the distribution range of the secondary stress around the borehole decreases with the decrease in the stress ratio, but the variation law is nonlinear. When the stress ratio is less than 0.5, the secondary stress distribution line around the borehole is similar to a straight line, indicating that the secondary stress in this area decreases very fast, so its influence range is small. When the stress ratio is in the range of 0.5~0.9, the secondary stress distribution line around the borehole is similar to the circular arc line, indicating that the secondary stress decline rate in this area gradually slows down, and the influence range gradually increases. When the stress ratio is greater than 0.9, the secondary stress around the borehole is affected by the borehole very little, so the area is very wide.

Taking the stress ratio of 0.5 as an example, Figure 1b shows that the distribution range of secondary stress around boreholes with different diameters is quite different. When the borehole diameter is less than 70 mm, the increment value of secondary stress distribution around boreholes is basically the same. With the increase in borehole diameter, the distribution range of secondary stress around boreholes also increases obviously. For

example, when the borehole diameter is 35 mm, the distribution range of secondary stress is about 50 mm. When the borehole diameter is 70 mm, the distribution range of secondary stress is about 100 mm, the borehole diameter increases by 35 mm, and the influence range of secondary stress increases by 50 mm. When the borehole diameter is greater than 70 mm, the secondary stress distribution around the borehole changes significantly, indicating that the stress increment increases significantly with the increase in the borehole diameter and also that the larger the borehole is, the wider the secondary stress distribution range is.

Figure 1c shows that the distribution of secondary stress around the borehole varies obviously with different borehole diameters. When the stress ratio is less than 0.5, the increase in the borehole diameter has little effect on the secondary stress distribution. With the increase in the stress ratio, the influence range of the increase in the borehole diameter on the secondary stress distribution increases gradually, and the increment of the shear influence range increases obviously. When the strain is relatively large, the increase in secondary stress around the borehole is more obvious. When the stress ratio is 0.3, the influence range of the borehole diameter of 35 mm is about 41 mm, the influence range of the borehole diameter of 70 mm is about 83 mm, and the influence range of the borehole diameter of 110 mm is about 131 mm. When the stress ratio is 0.78, the influence range of the borehole diameter of 35 mm is about 75 mm, the influence range of the borehole diameter of 70 mm is about 150 mm, and the influence range of the borehole diameter of 110 mm is about 234 mm. When the stress ratio is 0.98, the influence range of the borehole diameter 35 mm is about 245 mm, the influence range of the borehole diameter 70 mm is about 500 mm, and the influence range of the borehole diameter 110 mm is about 780 mm. It can be seen that different stress ratios have a significant effect on the secondary stress distribution of different diameter boreholes.

Figure 1d shows that different stress ratios have significantly different distribution areas around the borehole. When the stress ratio is below 0.75, the area of secondary stress distribution is about twice the diameter of the borehole. When the stress ratio increases to 0.9, the influence area of the secondary stress increases to about three times the diameter of the borehole. When the stress ratio increases to 0.98, the influence area of the secondary stress increases to about seven times the borehole diameter. The area of secondary stress distribution around the borehole is mainly concentrated in the range of twice the diameter of the borehole.

2.3. Establishment of Porosity Variation Model Under the Influence of Stress–Strain

Due to the secondary stress distribution around the coal seam borehole, the coal seam void volume will change [39].

The change in coal seam porosity around the borehole is as follows:

$$d\phi = d\left(\frac{V_p}{V_b}\right) = \frac{dV_p}{V_b} - \phi\frac{dV_b}{V_b} \tag{23}$$

where:

$$dV_p = -C_{pc}V_p d\sigma + C_{pp}V_p dp \tag{24}$$

$$dV_b = -C_{bc}V_b d\sigma + C_{bp}V_b dp \tag{25}$$

This is arranged as:

$$d\phi = -\phi C_{pc}d\sigma + \phi C_{pp}dp + \phi C_{bc}d\sigma - \phi C_{bp}V_b dp \tag{26}$$

Using the relationship between the compression coefficients, the relationship between porosity and stress is:

$$d\phi = -[C_{bc}(1-\phi) - C_s](d\sigma - dp) \tag{27}$$

Similarly, the expression of the volume strain is:

$$d\varepsilon_V = -\frac{dV_b}{V_b} = C_{bc}d\sigma - C_{bp}dp = C_{bc}(d\sigma - dp) + C_s dp \tag{28}$$

Therefore, the relationship between porosity and volume strain is:

$$d\varepsilon_V = -\left(1 - \frac{C_s}{C_{bc}} - \phi\right)(d\varepsilon_V - C_s dp) \tag{29}$$

This is arranged as:

$$\phi = 1 - \frac{C_s}{C_{bc}} + \frac{d\varepsilon_V}{d\varepsilon_V - C_s dp} \tag{30}$$

where ϕ is porosity; V_p is the physical examination of coal pores with a volume of V_b, m^3; V_b is the volume of coal, m^3; C is the compression coefficient; and p is the original rock stress, Mpa.

Equation (30) shows that when the compression coefficient of coal and gas and the original rock pressure of the coal seam are known, the change in porosity should become a similar inverse proportional function relationship with the body. When the coal body is in a compressed state, that is, greater than zero, the function is a decreasing function. When the coal body is in the expansion state, that is, less than zero, the function is an increasing function. Therefore, the pressure relief zone along the borehole is the coal body expansion zone, and the porosity increases with the increase in the strain in the pressure relief zone. The stress concentration zone is the coal body compression zone, and the porosity decreases with the increase in the strain in the stress concentration zone. In the original stress zone, the porosity of the region is unchanged because the coal body is not strained.

2.4. Establishment of Gas Migration Law Model Under the Condition of Stress–Seepage Coupling Field

Under the action of an in situ stress field, the secondary stress distribution will occur around the borehole. Affected by the secondary stress, the pressure relief zone, stress concentration zone, and original stress zone will be formed along the radial direction of the borehole. The porosity of each area around the borehole has also changed greatly. Due to the difference in porosity, the gas migration law around the coal seam gas pre-drainage borehole is divided into three parts. In the pressure relief area near the borehole center, the gas will undergo a fluid–solid coupling seepage process [40]. In the excessive flow area of stress concentration, the gas will undergo pipeline flow and molecular free flow, and the gas movement will be stagnant when it is close to the original rock stress area. Therefore, the stress–seepage coupling field model of the coal seam gas pre-drainage process includes the dynamic model of the fluid–solid coupling field and the pressure-driven pore flow model.

2.4.1. Establishment of Fluid–Solid Coupling Dynamic Model of Pressure Relief Zone Around Gas Drainage Boreholes

In the process of coal seam gas drainage, its motion process satisfies the gas continuity equation, gas motion equation, and gas state equation [1,2,41,42]. The above equations are combined to obtain:

$$\begin{cases} -\left[\frac{\partial(\rho_g v_x)}{\partial x} + \frac{\partial(\rho_g v_y)}{\partial y} + \frac{\partial(\rho_g v_z)}{\partial z}\right] = \frac{\partial(\phi\rho_g)}{\partial t} \\ v_x = -\frac{K}{\mu}\frac{\partial p}{\partial x} \\ v_y = -\frac{K}{\mu}\frac{\partial p}{\partial y} \\ v_z = -\frac{K}{\mu}\frac{\partial p}{\partial z} \\ pV = nZRT \end{cases} \tag{31}$$

Considering the viscosity and compression factor of real gas, the above equation is solved, and the seepage differential equation of gas can be obtained as follows:

$$\frac{\partial}{\partial x}\left[\frac{p}{\mu(p)Z(p)}\frac{\partial p}{\partial x}\right]+\frac{\partial}{\partial y}\left[\frac{p}{\mu(p)Z(p)}\frac{\partial p}{\partial y}\right]+\frac{\partial}{\partial z}\left[\frac{p}{\mu(p)Z(p)}\frac{\partial p}{\partial z}\right]=\frac{\phi}{K}\frac{\partial}{\partial t}\left[\frac{p}{Z(p)}\right] \tag{32}$$

The upper right side is:

$$\frac{\partial}{\partial t}\left[\frac{p}{Z(p)}\right]=\left[\frac{1}{p}-\frac{1}{Z(p)}\frac{\partial p}{\partial Z(p)}\right]\cdot\frac{p}{Z(p)}\frac{\partial p}{\partial t}=C(p)\frac{p}{Z(p)}\frac{\partial p}{\partial t} \tag{33}$$

This is arranged as:

$$\nabla\left[\frac{p}{\mu(p)Z(p)}\nabla p\right]=\frac{\phi\mu(p)C(p)}{K}\left[\frac{p}{\mu(p)Z(p)}\frac{\partial p}{\partial t}\right] \tag{34}$$

2.4.2. Establishment of Channel Flow Model in Stress Concentration Area Around Gas Drainage Borehole

The stress concentration zone around the borehole can be subdivided into the over-flow zone and the free-flow zone. It is assumed that the velocity distribution of the pressure-driven over-flow zone and the free-flow zone is parabolic, and the slip velocity can be expressed as follows:

$$U_s-U_w=\frac{2-\sigma_r}{\sigma_r}\left[\frac{K_n}{1-bK_n}\left(\frac{\partial U}{\partial n}\right)_s\right] \tag{35}$$

The dimensionless velocity scaling equation of micro-porous flow can be obtained:

$$U^*(r,K_n)=\frac{U(x,r)}{\overline{U(x)}}=\left[\frac{-\left(\frac{r}{d}\right)^2+1+2\times\frac{K_n}{1-bK_n}}{\frac{1}{2}+2\times\frac{K_n}{1-bK_n}}\right] \tag{36}$$

where d is the aperture, and then the volume flow rate in the hole is:

$$\dot{Q}=-\frac{\pi d^4}{8\mu_0}\times\frac{dp}{dx}(1-dK_n)\left(1+\frac{4K_n}{1-bK_n}\right) \tag{37}$$

Since b = -1 can be determined from the linearized Boltzmann solution, the only parameter to be determined in the model is d. However, d should change from the zero value in the slip flow region to the constant asymptotic value d_0 in the molecular flow region. The asymptotic value of the mass flow rate at that time can be obtained by Equation (38).

$$d_{K_n\to\infty}\equiv d_0=\left[\frac{64}{3\pi\left(1-\frac{4}{b}\right)}\right] \tag{38}$$

The variation of d as a K_n function obtained from the numerical and experimental data is as follows:

$$d=d_0\frac{2}{\pi}tan^{-1}\left(d_1\overline{K_n^{\beta}}\right) \tag{39}$$

The volume flow rate of the channel flow in the excessive flow area is:

$$\dot{Q}=C(AR)\frac{wh^3}{12\mu}\left(-\frac{dp}{dx}\right) \tag{40}$$

The volume flow rate of the rarefied gas flow in the molecular flow region is:

$$\dot{Q} = C(AR)\frac{wh^3}{12\mu_0} \times \left(-\frac{dp}{dx}\right)(1 + \alpha K_n)\left(1 + \frac{6K_n}{1 - 6K_n}\right) \quad (41)$$

where $C(AR)$ is the correction factor, generally taking 1 in the micro-pore flow.

So far, the mathematical model of the gas migration law under the condition of the stress–seepage coupling field in the coal seam gas pre-drainage process has been established.

In this model, ρ is the gas density, Kg/m^3; v is speed, m/s; K is permeability, m^2; μ is the viscosity coefficient, Pa·s; K_n is the number of effort; p is pressure, Pa; Vis volume, m^3; n is the amount of gas substance, mol; R is a gas constant, Pa·m^3/(mol·K); T is temperature, K; Z is the gas compression factor.

3. Numerical Simulation and Result Analysis

The difference of the drainage technology in the gas control of a high-gas and extra-thick coal seam is directly related to the safety and overall progress requirements of the mining work. In view of the complexity and non-repeatability of the coal seam gas drainage system, the CFD commercial software Fluent is used to numerically simulate the gas migration law of a pre-drainage coal seam in the fully mechanized caving face. The CFD simulation study is used to obtain a numerical solution of the fluid flow control equation. It obtains the mathematical description of the overall flow field concerned by solving the space–time solution. The basis of CFD is to establish the Navier–Stokes equation. It is composed of a series of partial differential equations describing the conservation law of fluid flow, and the conservation equations of mass and momentum are solved. The software has the ability to simulate complex flow fields from incompressible to highly compressible. ANSYS Fluent 6.3.26 contains a very rich physical model that can simulate complex multiphase flow. The model of the gas migration law based on a stress coupling field is also solved by the mass conservation equation of fluid flow. ANSYS Fluent 6.3.26 has powerful operation energy to simulate the law of fluid flow in porous media and is widely used in simulating the law of gas migration in goaf. In this section, the numerical simulation method is used to simulate the gas drainage control range and drainage effect by using computer technology. The core is to study the migration law of gas under different coal seam geologies and occurrence conditions, study the distribution law of gas movement under different boundary conditions, and study the main factors affecting the gas accumulation in fully mechanized caving mining so as to provide a basis and guidance for the application of gas disaster control technology in fully mechanized caving mining.

3.1. The Establishment of a Geometric Model and the Determination of Model Parameters

Taking a mine in Shanxi as an example, the coal seam occurrence conditions and gas parameters of the mine are shown in Table 1. Under the condition of ignoring the borehole pressure loss, the gas migration process and pressure change law of any section perpendicular to the borehole axis are the same. Combined with the secondary stress distribution law of the coal seam after drilling, the length is 150 m, the width is 50 m, and the height is 6.31 m. For a cuboid geometric model with a borehole diameter of 0.12 m, the schematic diagram of the coal seam drainage borehole is shown in Figure 2, and the geometric simulation is shown in Figure 3.

Table 1. Coal seam occurrence conditions and gas parameters.

Parameter	Value
Coal seam thickness	6.36 m
Gas emission quantity	67.62 m^3/min
Initial stress σ/MPa	13.5 MPa
Radius of drill hole r_0/m	0.06 m
Coal seam permeability coefficient	0.0605~0.1209 m^2/MPa^2d
Coefficient of kinetic viscosity μ/Pa·s	11.2×10^{-6}
Initial void ψ_0	0.09
Initial gas pressure p_0/MPa	0.17
Adsorption constants a/m^3·t^{-1}	23.925
Adsorption constants b/m^3·t^{-1}	0.319
Coal density ρs/t·m^{-3}	1.39
Universal gas constant R/(J·(mol·K)$^{-1}$)	8.3143
Absolute temperature T/K	300
Gas molar volume n/m^3·mol^{-1}	0.0224

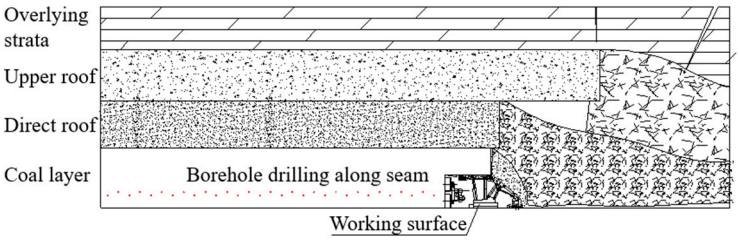

Figure 2. Pre-drainage coal seam gas drainage schematic diagram.

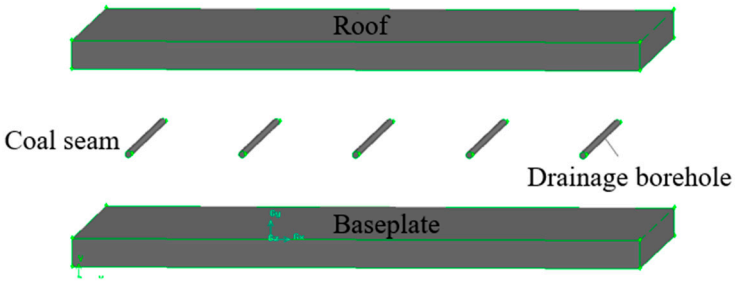

Figure 3. Geometric model of gas drainage in pre-drainage coal seam.

The setting of the boundary conditions mainly considers the porosity of the pre-drainage coal seam, the amount of gas analysis, the pre-drainage negative pressure, the pre-drainage borehole diameter, etc. The gas drilling in the coal seam is a kind of internal boundary condition for the simulation of gas drainage in the coal seam. When the gas drainage amount of the pre-drainage borehole is given, the known source and sink terms need to be supplemented in the gas motion equation. When the gas flow pressure of the pre-drainage borehole is given, it can be treated as a stable flow. The borehole flow pressure is usually known in the study of coal seam drainage. According to the relevant parameters of Table 1, the geometric area grid of the pre-drainage model is adjusted adaptively, and the numerical simulation parameters of the gas migration law of the pre-drainage coal seam are shown in Table 2.

Table 2. Simulation parameters of gas drainage in pre-drainage coal seam.

Simulated Condition	Simulation Parameters
Equation solver	Separation solver
Turbulent flow model	κ-ε two equations model
Component model	Gas
Energy model	Open
Convergence criteria	10^{-3}
Porous media model	Open
Percentage of void	0.09
Inertial resistance coefficient ($1/m^2$)	1.0×10^6
Pressure inlet (MPa)	0.17
Pressure outlet (KPa)	5

3.2. Simulation Study on Variation Law of Gas Pressure Under Different Aperture Conditions

Taking the relevant parameters of Tables 1 and 2 as the boundary conditions, the gas drainage process of 10 groups of boreholes, φ35, φ40, φ47, φ50, φ60, φ70, φ80, φ94, φ100, and φ120, is simulated. The gas pressure changes around the boreholes with diameters of φ70, φ80, φ94, φ100, and φ120 are shown in Figure 4, and the gas pressure changes around the boreholes with diameters of φ35, φ40, φ47, φ50, and φ60 are shown in Figure 5.

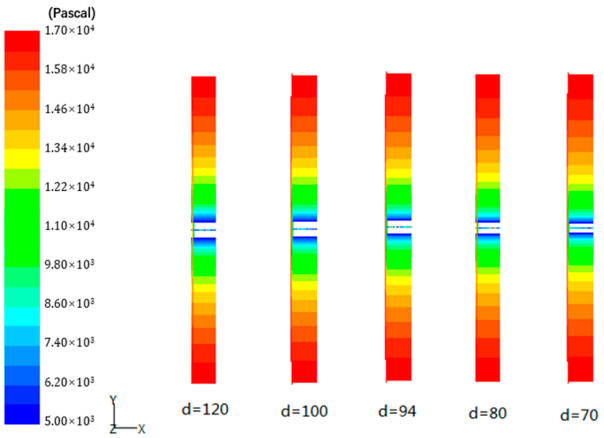

Figure 4. Gas pressure change cloud around different borehole diameters.

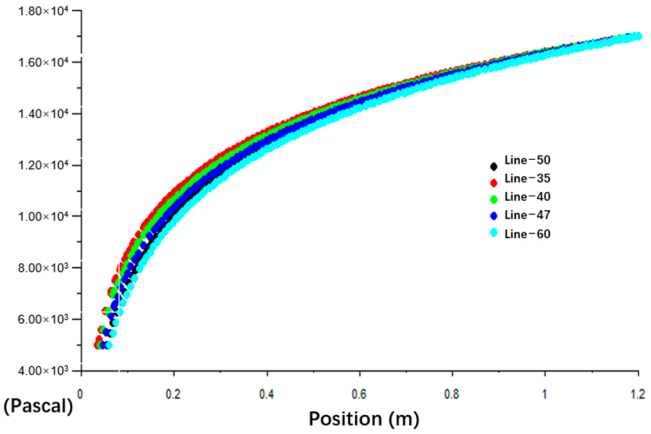

Figure 5. Gas pressure curves around different borehole diameters.

Figure 4 shows that due to the large borehole diameters, which are 70 mm, 80 mm, 94 mm, 100 mm, and 120 mm, the secondary distribution of stress around the borehole is very obvious. From Figure 4, the area range of the static pressure distribution can be clearly distinguished. Through the gas pressure distribution diagram around different

boreholes, it can be seen that the size of the aperture has a different influence range on the surrounding gas pressure, and the influence range gradually increases with the increase in the borehole. The variation law of the borehole and gas pressure shown in this diagram is basically consistent with that in Figure 1, which also indirectly proves the reliability of the secondary distribution model of the stress field of the coal body around the borehole. Figure 5 shows that under the influence of drilling and drainage negative pressure, when the borehole aperture is small, as shown in Figure 5, where the aperture is 35 mm, 40 mm, 47 mm, 50 mm, and 60 mm, the gas pressure around the borehole also changes, but its influence range is small, and its influence range has little to do with the size of the borehole aperture, generally not more than 1–2 times the diameter of the borehole. The simulation results also show that the borehole must not be too small during the pre-drainage of the coal seam gas; otherwise, it will affect the drainage effect of the coal seam gas.

3.3. Simulation Study on Variation Law of Gas Pressure Under Different Permeability Conditions

Due to the different degrees of metamorphism, the permeability of the coal body also shows great differences. Under the condition that other conditions remain unchanged, a gas drainage simulation study was carried out on the three groups of coal seams with resistance viscosity coefficients of 3.54×10^{17}, 3.54×10^{13}, and 3.54×10^{9}. The change law of gas pressure around it is shown in Figures 6 and 7.

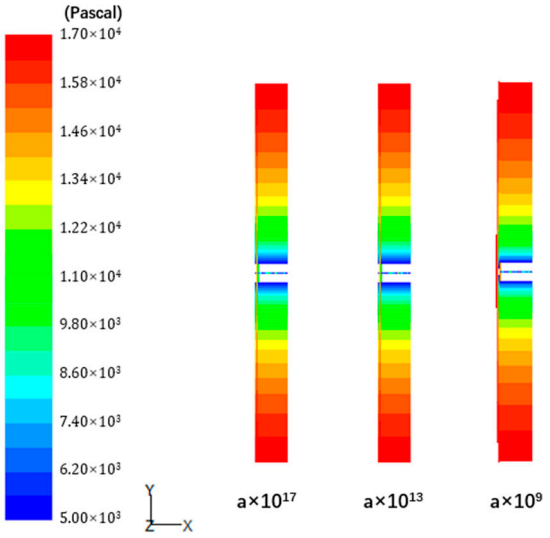

Figure 6. The pressure change cloud diagram around the aperture under different viscous resistance coefficients.

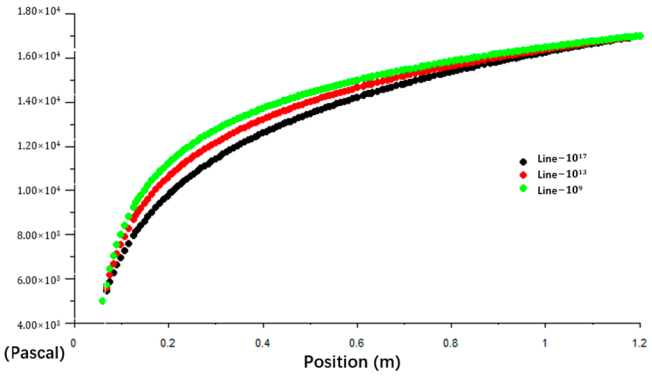

Figure 7. Pressure curves around the aperture under different viscous resistance coefficients.

Figures 6 and 7 show that the variation range of gas pressure around the borehole in the coal seam with good permeability is obviously larger than that in the coal seam

with poor permeability. The variation range of gas pressure in the coal seam with good permeability is 1.7 m, while that in the coal seam with poor permeability is only 1.0 m. In the coal seam with good permeability, the change rate of gas pressure around the borehole is significantly higher than that in the coal seam with poor permeability. However, when the gas pressure drops to a certain range, the change rate of gas pressure becomes significantly weaker and eventually tends to be stable.

3.4. Simulation Study on Variation Law of Borehole Gas Pressure Under Different Initial Pressure Conditions

Due to the different occurrence conditions of coal seams, the original pressure of gas varies greatly. Under the condition that other parameters remain unchanged, the inlet pressure, P = 0.17 MPa, P = 0.5 MPa, P = 1.0 MPa, P = 1.5 MPa, and P = 2.0 MPa, is changed to simulate the pressure change law around the borehole under different original gas pressures. The change cloud diagram and curve diagram are shown in Figures 8 and 9.

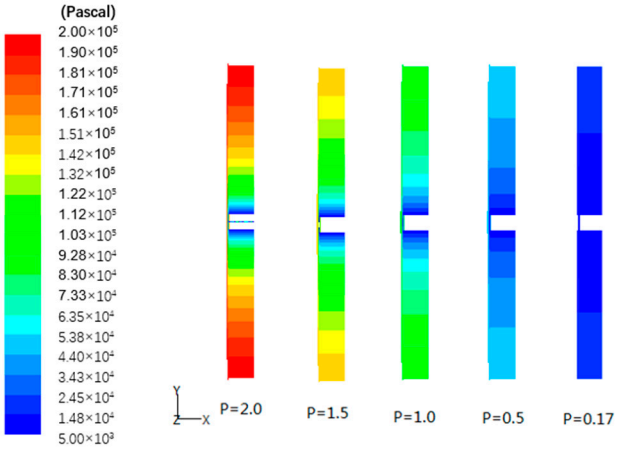

Figure 8. Pressure cloud diagram around the aperture under different original gas pressure.

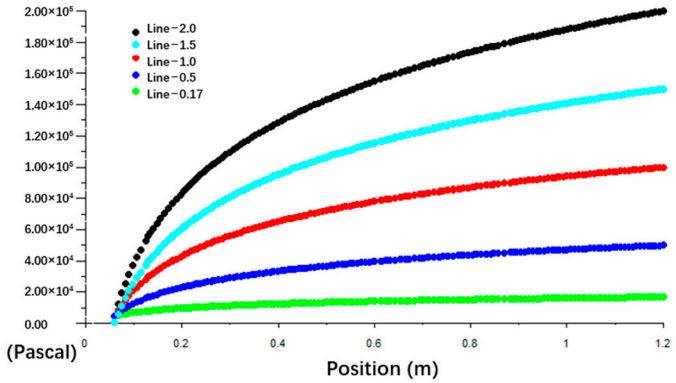

Figure 9. Pressure curve around the aperture under different original gas pressure.

Figures 8 and 9 show that the greater the original gas pressure, the greater the influence range of the gas pressure around the borehole, and the smaller the original gas pressure, the smaller the influence range of the gas pressure around the borehole; in the range of 0.4 m around the borehole, the pressure change rate gradually increases with the increase in the original gas pressure, indicating that the gas pressure attenuates rapidly under the same conditions. The influence range of gas pressure around all boreholes does not change linearly with the increase in the original pressure but changes in a curve law. Outside the 0.6 m around the borehole, the difference in the change rate of each curve gradually decreases, indicating that outside a certain range around the borehole, the original gas

pressure has little effect on the control range of the borehole, and its influence range is still limited.

Figures 10–13 show that when the pressure ratio is 0.98, the gas around the pre-drainage coal seam is affected by the secondary stress, and the gas migration in the coal seam of the porous medium is quite different. When the borehole is small, such as when the diameter of the borehole is 35 mm and 45 mm, the influence range of the secondary stress around the borehole is small, and the influence areas are not evenly distributed, so the gas migration speed changes significantly. With the increase in the diameter of the borehole, the influence range of the secondary stress around the borehole gradually increases, and the range of each partition also increases, while the gas migration speed in each region is more regionally stable.

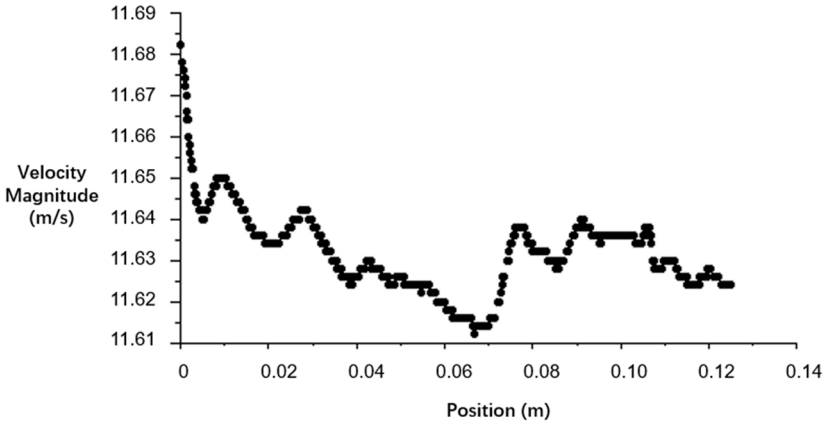

Figure 10. Gas migration velocity curve when the aperture is 35 mm and the pressure ratio is in the range of 0.98.

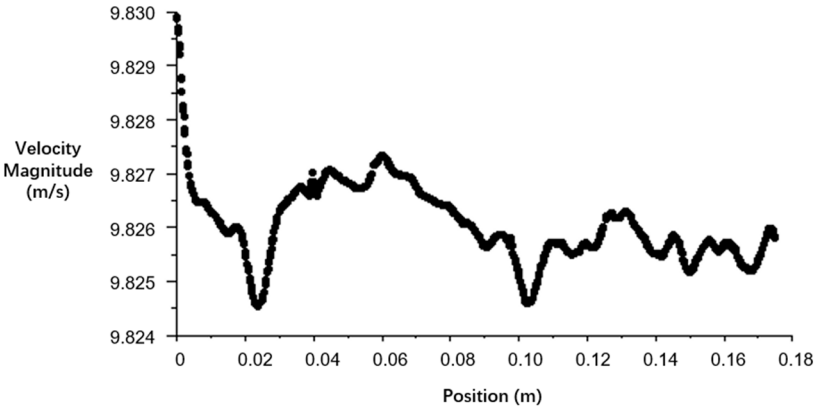

Figure 11. Gas migration velocity curve when the aperture is 50 mm and the pressure ratio is in the range of 0.98.

Figures 12 and 14–16 show that when the diameter of the borehole is the same, the pressure ratio around the borehole is different, so that the pressure of each pressure ratio area is different, and the deformation degree of the coal seam is also different. Therefore, the closer to the center of the borehole, the better the permeability of the coal seam, and the influence of the coal seam on the gas is gradually weakened. As shown in Figures 12 and 14–16, the smaller the pressure ratio, the faster the gas migration, and the more stable the operation. For example, when the pressure ratio drops to 0.3, the gas migration in the coal seam remains basically unchanged.

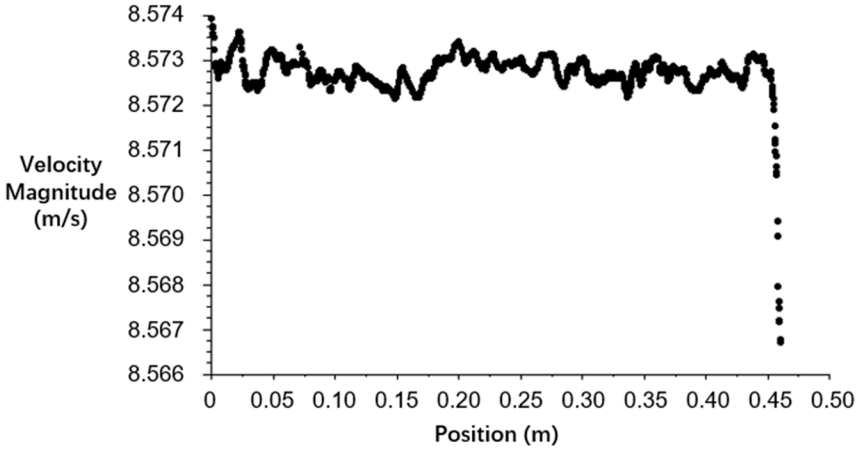

Figure 12. Gas migration velocity curve when the aperture is 65 mm and the pressure ratio is in the range of 0.98.

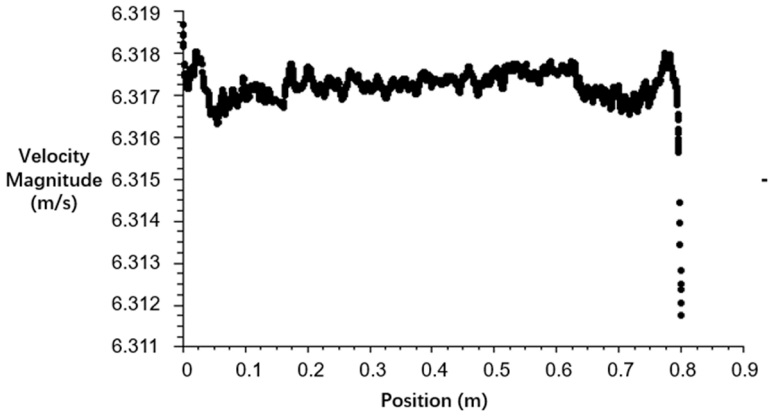

Figure 13. Gas migration velocity curve when the aperture is 80 mm and the pressure ratio is in the range of 0.98.

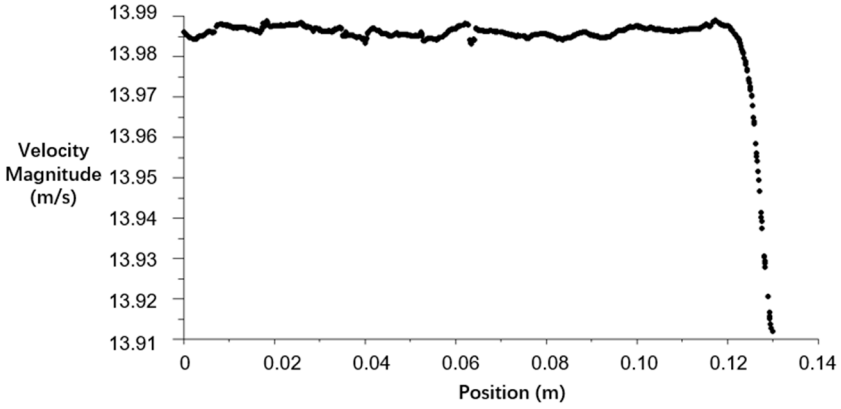

Figure 14. Gas migration velocity curve when the aperture is 65 mm and the pressure ratio is in the range of 0.75.

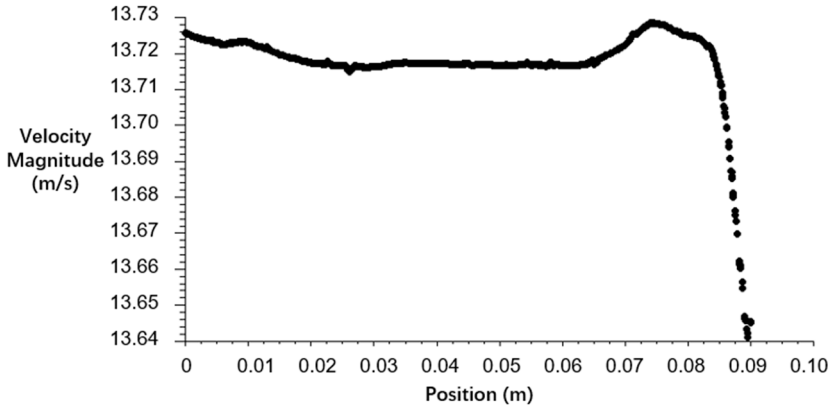

Figure 15. Gas migration velocity curve when the aperture is 65 mm and the pressure ratio is in the range of 0.5.

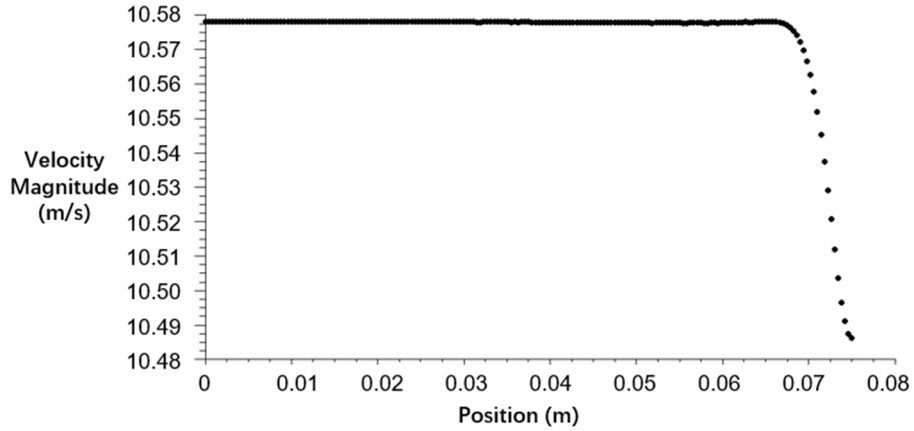

Figure 16. Gas migration velocity curve when the aperture is 65 mm and the pressure ratio is in the range of 0.3.

3.5. Analysis of Influencing Factors of Pre-Drainage Borehole Control Range

Generally speaking, the physical properties of coal, the borehole diameter, and the environment of the coal seam have a significant influence on the evolution of the flow field in the process of gas drainage. This section discusses the influence of borehole diameter, coal seam permeability, and gas original pressure on the control range, which will help to arrange gas drainage boreholes accurately and reasonably on site.

Borehole diameter. The influence range of the borehole is generally not more than 6~7 times the aperture. When the borehole aperture is 70 mm, the pressure influence range is 0.45 m, and the pressure influence range is 0.6 m when the aperture is 120 mm. The closer to the center of the borehole, the greater the change rate of the gas pressure, and the farther away from the center of the borehole, the smaller the change rate of the gas pressure, gradually approaching 0.

Coal seam permeability. The permeability of the coal seam is an important index in measuring the difficulty of gas drainage, and its control range is about 1.0~1.7 m. When the permeability of the coal seam is good, the gas pressure drop rate is small, and the drilling control range is large. When the permeability of the coal seam is poor, the gas pressure drop rate is large, and the drilling control range is small.

Gas original pressure. The control range of the gas drainage borehole and the original pressure of the gas change is a curve law. The higher the original pressure of the gas is, the larger the radius of the gas drainage is. A different original gas pressure will cause different gas pressure drop rates. In the range of 0.4 m around the borehole, the change rate of the pressure drop curve is larger. Outside 0.6 m around the borehole, the change rate of each curve tends to be consistent.

4. Field Practice and Effect Verification

In the study of the gas control effect in high-gas and extra-thick coal seams, field practice and effect verification are important links to ensure coal mine safety and efficient mining. First of all, according to the geological conditions of an extra-thick coal seam, a detailed mine gas composition analysis and pressure tests should be carried out to evaluate the gas content and its release characteristics. In the design of the drainage system, the combination of multi-point drainage and centralized drainage is usually used to achieve efficient gas removal. In the actual operation, by setting up multiple drainage holes, selecting the appropriate hole spacing and depth, and combined with the real-time monitoring system, the drainage parameters are dynamically adjusted. In this process, the gas drainage rate and the gas emission effect of the coal seam are the main assessment indicators.

The average thickness of the xxxx working face of a mine is 6.36 m. The initial stage of extraction is designed as a single row of gas extraction along the layer, and the diameter of the borehole is 70 mm. After a period of drainage, it is found that the gas drainage rate is low and the pre-drainage time is long, which cannot meet the production needs. After that, the gas drainage borehole is changed to 94 mm, and the upward and downward boreholes are arranged along the inclined direction of the working face in the belt crossheading and the auxiliary transportation crossheading, respectively. That is, half of the boreholes are parallel to the working face, and the other half of the boreholes have a certain angle with the working face and the horizontal plane. The two boreholes are alternately arranged to form a cross between the boreholes, as shown in Figure 17. According to the simulation results, the drilling control range is 0.7 m. When the cross hole is used, 70% of the coal seam can be within the drilling control range, so the drainage effect is obvious. Taking xxxx working face drainage in March 2013 as an example, the monthly gas drainage volume is 122,457 m^3, the daily maximum drainage volume is 6295 m^3, the minimum drainage volume is 2664 m^3, and the average drainage volume is 4479.5 m^3. The gas drainage rate reached 51.7%, and the pre-drainage time was greatly shortened. The drainage volume statistics are shown in Table 3.

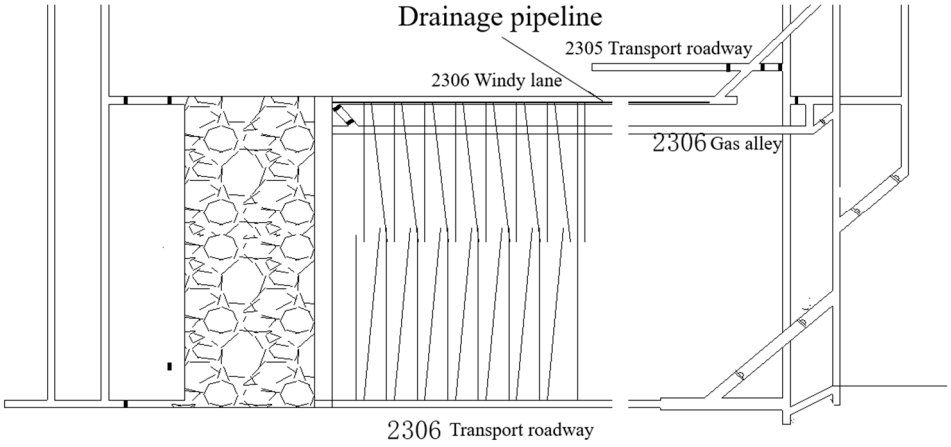

Figure 17. Working face drilling layout diagram.

The field data show that the optimized drainage design can effectively reduce the gas concentration in the coal seam and improve the safety factor. In the aspect of effect verification, the influence of gas drainage on mine safety and operation efficiency is evaluated by a comparison with the traditional drainage method. The measured results show that the newly designed drainage system not only effectively improves the gas drainage efficiency but also significantly reduces the risk of gas accidents, ensuring the safety of workers and the normal production of coal mines. In addition, the on-site feedback and continuous monitoring data provide a valuable basis for the subsequent optimization of the drainage scheme, forming a benign cycle improvement mechanism.

Table 3. Gas drainage statistics of xxxx working face in a mine.

Working Surface	Return Laneway		Tile Discharge Roadway		Upper Corner	Gas Drainage Volume (m^3/month)	Primitive Gas Content (m^3/t)	Residual Gas Content (m^3/t)	Drainage Rate (%)
	Wind Rate (m^3/min)	CH4 Average Concentration (%)	Wind Rate (m^3/min)	CH4 Average Concentration (%)	CH4 Average Concentration (%)				
xxxx	1120	0.39	310	0.54	0.45	122,457	5.53	2.67	51.7

Through the above practice and verification, the gas drainage design of a high-gas, extra-thick coal seam has achieved remarkable results in practical application, which provides a solid guarantee for safe coal mining. The results also further verify the reliability and accuracy of the numerical simulation results, which also show that the numerical simulation results can be used as a theoretical basis and reference for the gas drainage design of high-gas and extra-thick coal seams.

5. Discussion

This paper is based on the secondary distribution of coal seam stress around the borehole due to the influence of the borehole on the pre-drainage coal seam, which leads to the change in the porosity of the coal body around the borehole. Through theoretical analysis, the effect of borehole pre-drainage of coal seam gas control in the stress–seepage coupling field is studied in combination with the change in porosity around the borehole. The reliability and accuracy of the numerical simulation results are verified by the field-measured data. However, in view of the characteristics of complex coal seam occurrence conditions, large mining intensity, and many gas sources in fully mechanized top-coal caving mining, combined with the arduousness and urgency of gas disaster prevention and control technology development and research, there are still some key problems to be explored and discussed:

(1) In the process of high-gas coal seam mining, borehole drainage as an effective means of gas control has attracted extensive research attention. Based on the theoretical framework of the stress–seepage coupling field, this study deeply discusses the gas control effect of a borehole pre-drainage coal seam. The coupling relationship between stress and seepage has an important influence on the gas flow characteristics of the coal seam. Borehole drainage not only changes the pressure state in the coal seam but also significantly affects the release and migration mechanism of gas.

(2) Through the combination of numerical simulation and field practice data, we found that under different borehole apertures, coal seam permeabilities, and gas original pressures, the pre-drainage control range of boreholes shows obvious differences. In addition, the application of the stress–seepage coupling model enables us to predict the gas control effect under different drainage schemes more accurately, which provides a scientific basis for the safe mining of coal mines.

(3) In the practical application, the research results of the coupling model provide theoretical support for optimizing borehole drainage parameters and promote the development of gas control technology. However, it is still necessary to further study the drainage effect under different geological conditions and coal seam characteristics so as to provide more detailed guidance and reference for the production practice of coal mines. Future research should combine more field experiments and data analysis to verify the reliability of the theoretical model and explore more efficient gas control strategies.

6. Conclusions

Based on the theoretical analysis, this paper establishes a secondary distribution model of the stress field of a coal body around a borehole and a porosity change law model under the influence of stress–strain, The numerical simulation method is used to analyze the influence of different borehole diameters, different permeabilities, and different initial pressures on the gas pressure distribution around the coal seam borehole. According to the

field-measured data, the mathematical model of the gas migration law in fully mechanized top-coal mining is verified. The simulation results have guiding significance for the study of gas control technology. The main conclusions are as follows:

(1) The law of secondary stress redistribution around the borehole and its influence range are given. The size of the coal seam stress, to a certain extent, reflects the depth of the coal seam. When the stress is large, the gas content and initial pressure of the coal seam are generally high, and the gas pressure around the borehole changes in a large range, but the larger ground stress will also affect the permeability of the coal seam. When the permeability decreases, the range of gas pressure around the borehole will also decrease.

(2) Under the premise of considering the influence of stress and strain around the borehole, a fluid–solid coupling model of the seepage zone based on different porosities around the borehole, a pressure-driven transition flow zone, and a free molecular flow zone were established. The model combines the in situ stress and the change in porosity around the borehole, which makes the simulation more objective and specific. The permeability of a coal seam is an important index in measuring the difficulty of gas drainage. When the permeability of a coal seam is good, the gas pressure drop rate is small and the drilling control range is large. When the permeability of a coal seam is poor, the gas pressure drop rate is large and the drilling control range is small.

(3) The simulation results of the influence of the borehole diameter, the permeability of the coal seam, and the original gas pressure on the control range of the gas drainage borehole in the pre-drainage coal seam after the secondary stress distribution around the borehole are compared and analyzed, which provides a theoretical basis for the selection of the gas process parameters of the pre-drainage coal seam in the coal mine.

(4) The effective control range of drilling is that the gas pressure of the coal seam is reduced to 30~50% of the original pressure. It is considered that the better the permeability of the coal seam is, the higher the original pressure of the gas is, the larger the aperture of the gas drainage borehole is, the larger the control range of the gas drainage borehole is, the lower the density of the drainage borehole is, and the more obvious the drainage effect is.

Author Contributions: Formal analysis, writing—original draft preparation, H.W.; supervision, conceptualization, methodology, resources, H.A.; validation, formal analysis, investigation, B.Y. All authors have read and agreed to the published version of the manuscript.

Funding: This research was supported in part by the Yunnan Province "Caiyun" Postdoctoral Innovative Project Plan (No. CG24056E004A).

Institutional Review Board Statement: Not applicable.

Informed Consent Statement: Not applicable.

Data Availability Statement: Data are available from the corresponding author upon reasonable request.

Acknowledgments: The authors would like to express their sincere gratitude to the Kunming University of Science and Technology 2023 Undergraduate Education Teaching Reform Research Project (No. 075, KUST Education Office [2023]) for their support. Moreover, the authors would like to thank the anonymous reviewers for their valuable comments and constructive suggestions.

Conflicts of Interest: The authors declare no conflicts of interest.

References

1. Wang, H.; Jiang, J.; Wang, Z.Q.; Hu, G.Z.; Yuan, Z.G. Numerical simulation of seepage field of gas extraction drilling of single bedding of mining-coal bed. *Chongqing Daxue Xuebao/J. Chongqing Univ.* **2011**, *34*, 24–29.
2. Liu, Q.Q.; Cheng, Y.P.; Wang, H.F.; Liu, H.Y.; Liu, J.J. Numerical Resolving of Effective Methane Drainage Radius in Drill Hole along Seam. *Coal Min. Technol.* **2012**, *17*, 5–7.

3. Zhao, J.G. Construction technology and development tendency of high level directional driling in seam roof. *Coal Sci. Technol.* **2017**, *45*, 137–141.
4. Zhu, M. 3D simulation and control effect evaluation of gas extraction drilling in coal mine. *Min. Saf. Environ. Prot.* **2024**, *51*, 50–55. [CrossRef]
5. Terzaghi, K. *Theoretical Soil Mechanics*; John Wiley & Sons: Hoboken, NJ, USA, 1943; Volume 2, pp. 180–189. [CrossRef]
6. Biot, M.A. General theory of three-dimensional consolidation. *J. Appl. Phys.* **1941**, *12*, 155–164. [CrossRef]
7. Biot, M.A. Theory of elasticity and consolidation for a porous anisotropic solid. *J. Appl. Phys.* **1955**, *26*, 182–185. [CrossRef]
8. Biot, M.A. General Solutions of the Equations of Elasticity and Consolidation for a Porous Material. *J. Appl. Mech.* **1956**, *78*, 91–96. [CrossRef]
9. Lewis, R.W.; Roberts, P.J.; Schrefler, B.A. Finite element modelling of two-phase heat and fluid flow in deforming porous media. *Transp. Porous Media* **1989**, *4*, 319–334. [CrossRef]
10. Wang, H.; Dlugogorski, B.Z.; Kennedy, E.M. Pathways for Production of CO_2 and CO in Low-Temperature Oxidation of Coal. *Energy Fuels* **2003**, *17*, 150–158. [CrossRef]
11. Beamish, B.; Lau, A.; Moodie, A.; Vallance, T.A. Assessing the self-heating behaviour of Callide coal using a 2-metre column. *J. Loss Prev. Process Ind.* **2002**, *15*, 385–390. [CrossRef]
12. Harpalani, S.; Chen, G. Estimation of changes in fracture porosity of coal with gas emission. *Fuel* **1995**, *74*, 1491–1498. [CrossRef]
13. Lewis, R.; Sukirman, Y. Finite element modelling of three-phase flow in deforming saturated oil reservoirs. *Int. J. Numer. Anal. Methods Geomech.* **1993**, *17*, 577–598. [CrossRef]
14. Zhang, Z.G. Prediction of multi-borehole undermine coalbed gas drainage. *J. Coal Sci. Eng. (China)* **2009**, *15*, 295–298. [CrossRef]
15. Li, Z.L. New definition of correlation function with interval number and its application in extenics. *Math. Pract. Theory* **2006**, *36*, 207–210.
16. Shen, Z.; Zhang, X.; Sun, Y. Research on stress-seepage-damage coupling model of hydraulic fracturing for rock mass. *Jisuan Lixue Xuebao/Chin. J. Comput. Mech.* **2009**, *26*, 523–528.
17. Jasinge, D.; Ranjith, P.; Choi, S. Effects of effective stress changes on permeability of latrobe valley brown coal. *Fuel* **2011**, *90*, 1292–1300. [CrossRef]
18. Cao, J.; Dong, L.; Ai, D.; Wang, F.; Cui, Y.G. Nonlinear seepage law of deep hole water-injection in working face under the influence of mining. *J. China Coal Soc.* **2017**, *42*, 225–232.
19. Zhao, Y.; Lin, B.; Liu, T.; Zheng, Y.; Kong, J.; Li, Q.; Song, H. Mechanism of multifield coupling-induced outburst in mining-disturbed coal seam. *Fuel* **2020**, *272*, 117716. [CrossRef]
20. Liu, Z.; Hu, P.; Yang, H.; Yang, W.; Gu, Q. Coupling Mechanism of Coal Body Stress–Seepage around a Water Injection Borehole. *Sustainability* **2022**, *14*, 9599. [CrossRef]
21. Yuan, L.; Guo, H.; Shen, B.; Qu, Q.; Xue, J.-H. Circular overlying zone at longwall panel for efficient methane capture of mutiple coal seams with low permeability. *J. China Coal Soc.* **2011**, *36*, 365.
22. Hu, Q.T.; Liang, Y.P.; Liu, J.Z. CFD simulation of goaf gas flow patterns. *Meitan Xuebao/J. China Coal Soc.* **2007**, *32*, 719–723.
23. Li, S.-G.; Zhang, W.; Lin, H.-F. Numerical simulation on the delivery law of gob gas of fully mechanized caving face. *J. Coal Sci. Eng.* **2008**, *14*, 403–406. [CrossRef]
24. Zhang, T.; Li, W.; Li, S.; Song, S.; Tang, F. Gas emission law in high gas goaf of fully mechanized caving face. *Sci. Technol. Rev.* **2015**, *33*, 58–62. [CrossRef]
25. Wang, T.; Nie, C.; Yang, X.; Wang, P. Numerical simulation of gas drainage in gob considering temperature change. *Coal Sci. Technol.* **2021**, *49*, 85–94.
26. Hao, F.; Liu, M.; Sun, L.J. Determination method of gas drainage radius based on multi physics coupling. *J. China Coal Soc.* **2013**, *38* (Suppl. S1), 106–111.
27. Yang, T.H.; Chen, S.K.; Zhu, W.C.; Liu, H.L. Coupled Model of Gas-Solid in Coal Seams Based on Dynamic Process of Pressure Relief and Gas Drainage. *Rock Soil Mech.* **2010**, *31*, 2247–2252.
28. Ding, H.; Jiang, Z.; Han, Y. Numerical simulation and application of boreholes along coal seam for methane drainage. *Chin. J. Eng.* **2008**, *30*, 1205–1210.
29. Wang, Y.G.; Li, H.Y.; Qi, Q.X.; Peng, Y.W.; Li, C.R.; Deng, Z.G. The evolution of permeability and gas extraction technology in mining coal seam. *Meitan Xuebao/J. China Coal Soc.* **2010**, *35*, 406–410.
30. Furati, K.M. Effects of Relative Permeability History Dependence on Two-Phase Flow in Porous Media. *Transp. Porous Media* **1997**, *28*, 181–203. [CrossRef]
31. Bentsen, R.G. The Physical Origin of Interfacial Coupling in Two-Phase Flow through Porous Media. *Transp. Porous Media* **2001**, *44*, 109–122. [CrossRef]
32. Zhao, Y.-J.; Guo, H.-D.; Yuan, S.-J. The Study on the Key Gas Drainage Technique by Long & large Diameter Roof Boreholes in Fully Mechanized Face. *J. Taiyuan Univ. Technol.* **2009**, *40*, 74–77.
33. Ertekin, T.; King, G.A.; Schwerer, F.C. Dynamic Gas Slippage: A Unique Dual-Mechanism Approach to the Flow of Gas in Tight Formations. *Spe Form. Eval.* **1986**, *1*, 43–52. [CrossRef]
34. Ertekin, T.; Sung, W.; Schwerer, F.C. Production Performance Analysis of Horizontal Drainage Wells for the Degasification of Coal Seams. *J. Pet. Technol.* **1988**, *40*, 625–632. [CrossRef]

35. Smith, D.M.; Williams, F.L. Diffusional effects in the recovery of methane from coalbeds. *Soc. Pet. Eng. J.* **1984**, *24*, 529–535. [CrossRef]
36. Ancell, K.; Lambert, S.; Johnson, F.S. Analysis of the coalbed degasification process at a seventeen well pattern in the Warrior Basin of Alabama. In *SPE Unconventional Gas Recovery Symposium*; SPE: Pittsburgh, PA, USA, 1980. [CrossRef]
37. Guo, Y.S.; Lin, B.Q.; Wu, C.S. Coupling relation of crack evolvement in surrounding rocks with the storage and migration of mining induced releasing gas. *J. Min. Saf. Eng.* **2007**, *24*, 4.
38. Liu, Z.; Li, Z.; Yang, Y.; Ji, H. Experimental study of effect of water on sorption and radial gas seepage of coal. *Yanshilixue Yu Gongcheng Xuebao/Chin. J. Rock Mech. Eng.* **2014**, *33*, 586–593.
39. Tao, Y.; Xu, J.; Cheng, M.; Li, S.; Peng, S. Theoretical analysis and experimental study on permeability of gas-bearing coal. *Yanshilixue Yu Gongcheng Xuebao/Chin. J. Rock Mech. Eng.* **2009**, *28*, 3363–3370.
40. Yin, G.-Z.; Li, M.; Li, S.-Z.; Li, W.; Yao, J.-W.; Zhang, Q. 3D numerical simulation of gas drainage from boreholes based on solid gas coupling model of coal containing gas. *J. China Coal Soc.* **2013**, *38*, 535–541.
41. Ju, L. Solid-Gas Coupling Dynamics Model and It's Application Research of Coal Containing Gas. *China Min. Mag.* **2013**, *22*, 126–131.
42. Si, H.; Guo, T.; Li, X.H. Analysis and numerical simulation of fluid-structure coupling of gas drainage from boreholes. *J. Chongqing Univ. (Nat. Sci.)* **2011**, *34*, 105–110.